



Article

Modeling Brittle-to-Ductile Transitions in Rock Masses: Integrating the Geological Strength Index with the Hoek–Brown Criterion

Balázs Vásárhelyi ^{1,*}, Samad Narimani ¹, Seyed Morteza Davarpanah ² and Gábor Mocsár ³

¹ Department of Engineering Geology and Geotechnics, Faculty of Civil Engineering, Budapest University of Technology and Economics, 1111 Budapest, Hungary; samadnarimani@edu.bme.hu

² Research Institute of Mines and Environment (RIME), Université du Québec en

Abitibi-Témiscamingue (UQAT), Rouyn-Noranda, QC J9X5E4, Canada; seyedmorteza.davarpanah@uqat.ca

³ Department of Oncoradiology, Faculty of Medicine, University of Debrecen, 4032 Debrecen, Hungary; mocsgab@gmail.com

* Correspondence: vasarhelyi.balazs@emk.bme.hu

Abstract: Many studies focus on brittle–ductile transition stress in intact rocks; however, in real life, we deal with rock mass which contains many discontinuities. To fill this gap, this research focuses on the brittle–ductile transition stress of rock mass by considering the influence of different Geological Strength Index (*GSI*) values on the brittle–ductile transition stress of rock mass. In other words, the Hoek–Brown failure criteria for rock mass were reformulated mathematically including the ductility parameter (*d*), which is defined as the ratio of differential stress to minor stress. Then, the results were analyzed and plotted between $\frac{\sigma_3^*}{\sigma_c}$ and *GSI*, considering different (*d*) and Hoek–Brown material constant (*m_i*) values. The brittle–ductile transition stress, σ_3^* , was determined by intersecting the Hoek–Brown failure envelope with Mogi’s line, with ductility parameters *d* ranging from 3.4 (silicate rocks) to 5.0 (carbonate rocks). Numerical solutions were derived for $\frac{\sigma_3^*}{\sigma_c}$ as a function of *GSI* using Matlab, and the results were fitted with an exponential model. The analysis revealed an exponential relationship between $\frac{\sigma_3^*}{\sigma_c}$ and *GSI* for values above 32, with accuracy better than 3%. Increased ductility reduces rock mass strength, with higher *d* values leading to lower $\frac{\sigma_3^*}{\sigma_c}$. The diminishing returns in confinement strength at higher *GSI* values suggest that rock masses with higher *GSI* can sustain more confinement but with reduced effectiveness as *GSI* increases. These findings provide a framework for predicting brittle–ductile transitions in rock engineering.

Keywords: rock mechanics; brittle–ductile transition; rock mass; Hoek–Brown criteria; geological strength index (*GSI*); Mogi’s line



Citation: Vásárhelyi, B.; Narimani, S.; Davarpanah, S.M.; Mocsár, G.

Modeling Brittle-to-Ductile

Transitions in Rock Masses:

Integrating the Geological Strength

Index with the Hoek–Brown Criterion.

Appl. Mech. **2024**, *5*, 634–645. [https://](https://doi.org/10.3390/applmech5040036)

doi.org/10.3390/applmech5040036

Received: 26 August 2024

Revised: 24 September 2024

Accepted: 28 September 2024

Published: 30 September 2024



Copyright: © 2024 by the authors. Licensee MDPI, Basel, Switzerland. This article is an open access article distributed under the terms and conditions of the Creative Commons Attribution (CC BY) license (<https://creativecommons.org/licenses/by/4.0/>).

1. Introduction

The brittle–ductile transition stress in the rock mass is crucial in understanding its mechanical behavior under varying conditions. Rocks exhibit two primary modes of deformation: brittle and ductile. In the brittle regime, rocks tend to fracture and fail through the propagation of cracks and fractures. This is characterized by a sudden release of stored elastic energy, resulting in a relatively rapid failure. In the field of rock mechanics, several researchers have characterized brittleness as a material’s propensity to fracture when subjected to stress, such as tension or compression, without undergoing significant or lasting deformation. This definition emphasizes that a brittle material can break suddenly, often with little warning, because it lacks the ability to absorb energy and deform plastically before failure. Such behavior is contrasted with ductile materials, which can undergo considerable deformation before fracturing. Brittleness is a critical factor in understanding how rocks and other materials will behave under different loading conditions, making it essential in various engineering and geological applications [1–3] (see Figure 1).

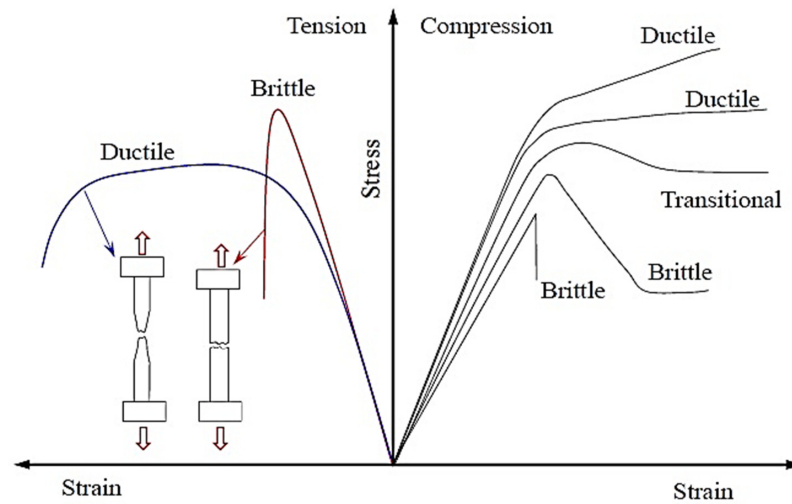


Figure 1. Brittle and ductile behavior under tension (left) and compression (right). The right side illustrates the rock’s behavior under varying confining pressures (based on [4]).

On the other hand, in the ductile regime, rocks deform without significant fracturing, showing plastic flow and a more gradual failure process [4]. The plastic deformation and post-peak behavior of rock mass are characterized by the brittle–ductile transition and nonlinear deformation behaviors, which are the prominent characteristics of the rocks. The transition occurs in failure mode from localized brittle fracture to non-localized plastic flow. This transition plays a significant role in various geophysical and geological problems [4].

Numerous experimental studies have shown that the failure behavior of rocks undergoes a transition from brittle to ductile as confining pressure increases [5,6]. The extent of brittleness is directly influenced by the level of confining stress, with rocks exhibiting significant brittleness under unconfined or low-pressure conditions. As the confining stress approaches the critical level near the brittle–ductile transition point, the rock’s behavior shifts towards being almost ductile. This progression is well-documented, as exemplified in a triaxial compression test performed on Tennessee marble by Wawersik and Fairhurst in 1970, which vividly contrasts the rock’s brittle and ductile responses under varying pressures (see Figure 2) [7].

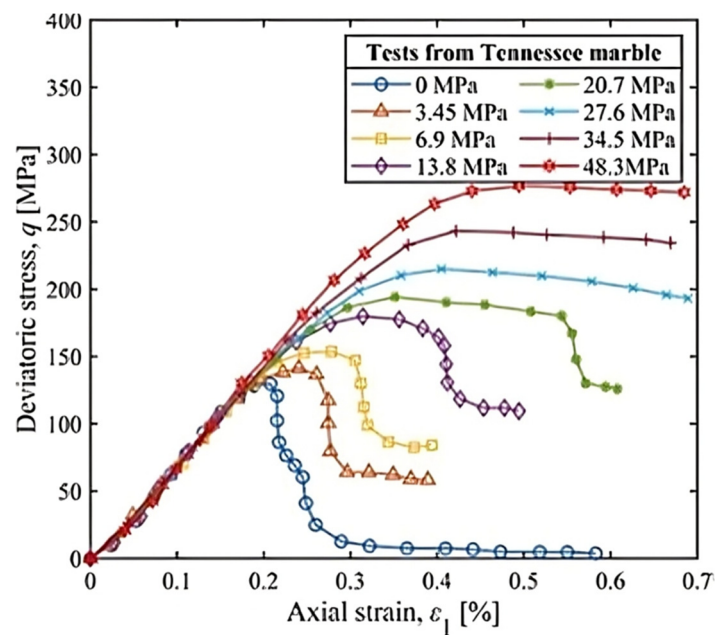


Figure 2. Stress–strain curves for Tennessee marble, where $q = \sigma_1 - \sigma_3$ (data after [7]).

Brittle failure occurs when a rock's resistance to load diminishes as deformation increases, while ductile behavior is marked by rising compressive strength with greater strain during compression tests. Reichmuth [8] and Lawn and Marshall [9] characterized brittleness as the ease with which cracks propagate. Dollinger et al. [10] described it as the tendency of rock to form chips during indentation. According to Lawn and Marshall [9], brittleness is one of the most complex mechanical properties, reflecting the interplay between deformation (such as residual or plastic impressions) and fracture under indentation.

Kármán [11–13] was the first who investigate the influence of the confining pressure on the mechanical behavior of intact rocks. Kármán [11,12] investigated the effect of the confining pressure of Mutenberg sandstone and Carrara marble. According to his laboratory results, the brittle material becomes ductile due to increasing the confining pressure. The pressure effect on rock strength is quite different between brittle and ductile fractures.

In many cases, a linear relationship between breaking strength and pressure has been observed [4,14–16]. On the other hand, Robertson [17] has shown that yield stress in ductile cases is practically independent of pressure in some limestones and marbles. Some rocks still exhibit brittleness even under high confining pressure at 1000 MPa or above [18].

The transition between these two states depends on various factors, including strain rate, temperature, effective stress, microstructure, porosity, and mineralogy of the rock and water [19–25]. Understanding the brittle–ductile transition stress is essential in geology and rock engineering. O'Ghaffari et al. [26] presented a novel method for unpicking the transitions in microphysical processes that accompany the macroscopic brittle–ductile transition. Their research provides exceptional time resolution and is able to distinguish among microcracking, twin formation, and dislocation activity, all in operando at the extreme conditions associated with rock deformation under higher confining pressure. Tang et al. [27] presented a strength-mapping method that relies on a mapping index formulated by plastic shear strains. This novel unified hardening/softening model has been successfully constructed, which can not only reflect the brittle failure characteristics of rock samples under lower confining pressure but also capture the transition from brittle to ductile behavior as the confining pressure increases. Understanding the brittle–ductile transition stress is essential in geology and rock engineering.

In geological contexts, it helps predict the behavior of rock formations under different tectonic conditions. In engineering, particularly in tunneling, mining, and underground construction, radioactive waste storage, and hydrogen storage. A significant amount of strain energy is stored in surrounding rocks following excavation. Brittle rocks, which deform minimally, consume only a small portion of this energy. Consequently, a large portion of the stored strain energy is converted into the kinetic energy of rock blocks during a rockburst. In contrast, ductile rocks experience considerable deformation due to squeezing and creep, which leads to nearly complete dissipation of strain energy. As a result, the degree of rock brittleness serves as a crucial indicator for predicting the likelihood of rockbursts in deep mining and tunneling operations [28–31].

Knowing the transition stress aids in designing support structures to withstand the specific mechanical properties of the rock mass. Researchers employ laboratory experiments, field studies, and numerical modeling to determine the transition stress for different rock types and conditions. This knowledge is crucial for ensuring the safety and stability of structures built within or on rock formations, contributing to the overall success of various engineering projects.

In rock masses with high Geological Strength Index (*GSI*) values (indicating fewer and less severe discontinuities), the transition from brittle to ductile behavior occurs at higher stresses. These rock masses can sustain more stress before transitioning to ductile deformation, as the intact rock strength dominates the behavior. Conversely, in rock masses with low *GSI* values (indicating more fractured and less coherent rock masses), the transition to ductile behavior occurs at lower stress levels, as the fractures and discontinuities weaken the rock mass, making it more prone to ductile deformation under lower stress. Thus, *GSI*

is crucial in determining the stress at which a rock mass will transition from brittle failure to ductile flow, affecting the stability and design of engineering structures in rock.

This paper investigates the brittle–ductile transition in rock masses by incorporating the influence of the Geological Strength Index (*GSI*) into the Hoek–Brown failure criterion. Traditional studies primarily focus on intact rock, often overlooking the discontinuities and heterogeneities present in actual rock masses. This research addresses that gap by reformulating the Hoek–Brown criterion to include a ductility parameter, defined as the ratio of differential stress to minor stress, to better represent real-world rock mass behavior.

This study explores how varying confining pressures lead to a transition from brittle to ductile behavior in rocks. Brittle failure is typically characterized by crack initiation and propagation, often resulting in sudden failure and energy release. In contrast, ductile behavior is marked by continuous deformation and plastic flow. The transition between these behaviors is influenced by factors such as confining stress and rock mass quality, with *GSI* playing a critical role. Numerical models and experimental data are used to demonstrate that as confining stress increases, rock behavior shifts from brittle to ductile. This study provides fitted models that approximate the behavior of rock masses during this transition, improving the prediction of rock mass responses in engineering applications.

2. Origin of the Geological Strength Index (*GSI*) in the Hoek–Brown Criterion

The Hoek–Brown failure criterion was initially developed to describe the failure of intact rock [22,32]:

$$\sigma_1 = \sigma_3 + \sigma_c \left(m_i \frac{\sigma_3}{\sigma_c} + 1 \right)^{0.5} \quad (1)$$

where σ_1 and σ_3 are the major and minor main stress, respectively, σ_c is the unconfined compressive strength and m_i is a material-dependent constant.

The following semi empirical failure criterion was introduced by Hoek and Brown for rock mass [33,34]:

$$\sigma_1 = \sigma_3 + \sigma_c \left(m_b \frac{\sigma_3}{\sigma_c} + s \right)^a \quad (2)$$

where σ_c is the uniaxial compressive strength of the intact rock, while a , m_b , and s depend on the Geological Strength Index (*GSI*), according to the following form:

$$a = \frac{1}{2} + \frac{1}{6} \left(e^{-\frac{GSI}{15}} - e^{-\frac{20}{3}} \right) \quad (3)$$

$$m_b = m_i e^{\frac{GSI-100}{28}} \quad (4)$$

where m_i is the Hoek–Brown material constant of intact rock,

$$s = e^{\frac{GSI-100}{9}} \quad (5)$$

The Geological Strength Index (*GSI*), according to the definition, can have a value between 0 (disturbed rock mass) and 100 (intact rock). *GSI* offers a way to estimate the mechanical properties of a rock mass (such as cohesion and friction angle) by classifying the rock mass based on its structure (e.g., blocky, massive, or highly fractured) and the condition of discontinuities (e.g., roughness, weathering, and infilling) [34].

As mentioned above, the Hoek–Brown criterion requires certain input parameters, such as the rock mass constant (m_i), the uniaxial compressive strength of intact rock (σ_{ci}), and a factor s representing the rock mass quality. *GSI* provides a practical way to estimate these parameters, particularly m_i and s , based on field observations of the rock mass. The *GSI* adjusts the Hoek–Brown parameters to reflect the influence of geological factors on rock mass behavior. As the *GSI* decreases (indicating poorer rock mass quality), the estimated rock mass strength and deformation parameters are reduced, this directly influences the predictions made by the Hoek–Brown criterion. This is crucial for designing safe and effective engineering structures in varying rock conditions [34].

The *GSI* system is often integrated with the Hoek–Brown criterion within rock mass classification schemes, such as the Rock Mass Rating (RMR) system. Together, they provide a comprehensive approach to estimating the mechanical behavior of complex rock masses, which is essential for stability analyses and design in rock engineering. The Hoek–Brown criterion provides a framework for understanding rock mass strength, and *GSI* is a practical tool that helps quantify the necessary parameters based on geological conditions. The two works together to offer a realistic assessment of rock mass behavior in engineering projects.

3. Ductility Parameter and Brittle–Ductile Transition Stress for Intact Rock

Mogi [4] suggested introducing the ductility parameter by the transition from shear to ductile failure. He found that the average transition is defined by $\sigma_1 = 3.4 \sigma_3$ (this is Mogi’s line). The variability in the confining pressure (σ_3) associated with the transition is given in Table 1, based on the data collected by Walton [35].

Table 1. Transition confining pressure of different rock types.

Rock Type	Confining Pressure [MPa]
Rock salt	0–17
Chalk	<10
Limestone	20–220
Sandstone	10–400
Granite	>>100

Walton [35] collected the ductility parameters of different rock types. Applying Mogi’s equation,

$$\sigma_1 - \sigma_3 = d\sigma_3 \tag{6}$$

where the ductility parameter (*d*) is an empirical parameter and it depends on the type of rock: it is between 0.9 (Green River Shale) and 10.7 (Jinping marble)—the average value for carbonates it is between 3.5 and 5.0; and for silicates it is between 2.0 and 3.5 [35]. In Figure 3, the compressive strength ($\sigma_1 - \sigma_3$) as a function of confining stress (σ_3) is plotted using the brittle–ductile transition data collection of Walton [35].

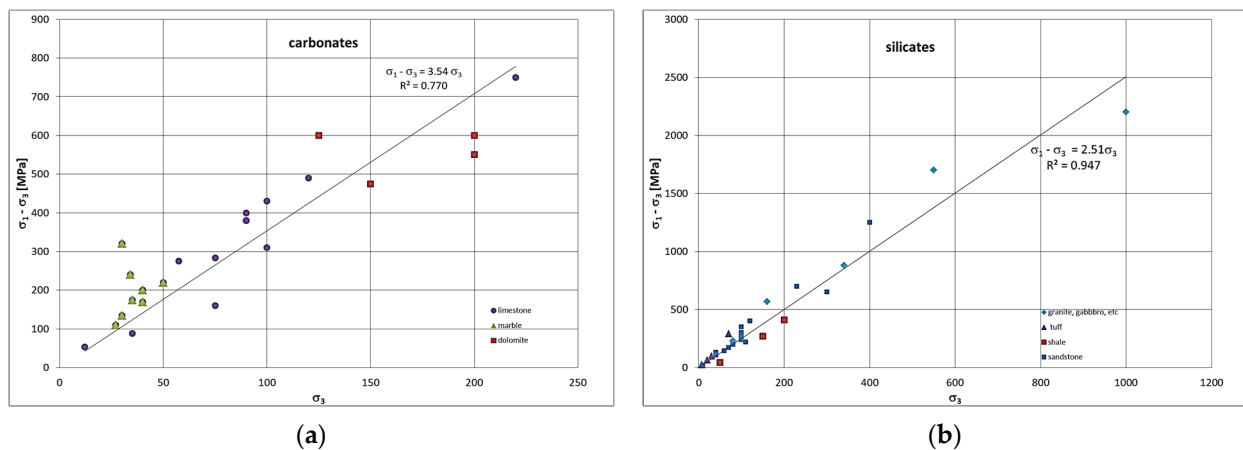


Figure 3. Compressive strength ($\sigma_1 - \sigma_3$) as a function of brittle–ductile transition stress (σ_3): (a) carbonate and (b) silicate rocks according to Walton’s data collection [35].

For calculating the confining stress at brittle–ductile transition, the following were assumed [35]:

- The Hoek–Brown failure envelope for intact rock can be used;
- Introducing the ductility parameter (*d*): $\sigma_1 = (d + 1) \sigma_3$.

Calculating the intersection of the two equations, the brittle–ductile transition occurs (σ_3^*):

$$\sigma_3^* = \frac{\sigma_c \left(m_i + \sqrt{m_i^2 + 4d^2} \right)}{2d^2} \tag{7}$$

According to Walton’s analysis [35] on the effects of fluid saturation, fluid saturation tends to decrease strength without significantly influencing brittleness, leading to a corresponding decrease in d .

Davarpanah et al. [36] also investigated the relationship between brittle–ductile transition stress and Hoek–Brown failure criteria for intact rock, calculating the intersection of the Hoek–Brown failure criteria and Mogi’s line for different types of rocks.

Figure 4 illustrates how the failure envelope changes with varying GSI values. Higher GSI values result in a steeper curve, indicating stronger rock mass conditions. The intersection points of the curves with Mogi’s line suggest transition stresses where failure criteria change, marking the thresholds under different GSI conditions.

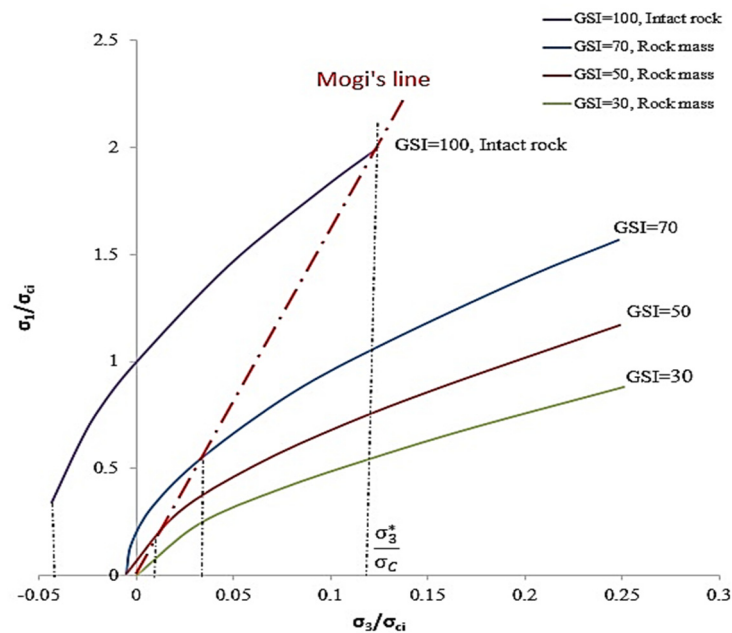


Figure 4. Relationship between Hoek–Brown failure envelopes with different GSI values, Mogi’s line, and different transition stresses.

Davarpanah et al. [36] suggest that, knowing the unconfined compressive strength (σ_c) and tensile strength (σ_t) [37], the brittle–ductile transitional confining stress can be determined as follows:

- Silicate rocks

$$\sigma_3^* = \sigma_c \frac{\left(\frac{\sigma_c}{\sigma_t} - 0.17 \right) \sqrt{\left(\frac{\sigma_c}{\sigma_t} - 0.17 \right)^2 + 46.24}}{23.12} \tag{8}$$

- Carbonate rocks

$$\sigma_3^* = \sigma_c \frac{\left(\frac{\sigma_c}{\sigma_t} - 0.17 \right) \sqrt{\left(\frac{\sigma_c}{\sigma_t} - 0.17 \right)^2 + 100}}{50} \tag{9}$$

4. Derivation of Confining Stress at the Brittle–Ductile Transition of Rock Mass

According to the suggestions of Mogi [4] and Walton [35] there is a linear relationship at the brittle–ductile transition, which constant is the ductility (d) value:

$$\sigma_1 - \sigma_3 = d\sigma_3 \tag{10}$$

It is equal to

$$\sigma_1 = (d + 1)\sigma_3 \tag{11}$$

It was assumed that the d parameter is independent on the rock mass quality and depends only on the rock type.

Substituting Equation (11) into Equation (2):

$$(d + 1)\sigma_3 = \sigma_3 + \sigma_c \left(m_b \frac{\sigma_3}{\sigma_c} + s \right)^\alpha \tag{12}$$

$$\frac{d\sigma_3}{\sigma_c} = \left(m_b \frac{\sigma_3}{\sigma_c} + s \right)^\alpha \tag{13}$$

$$\left(\frac{d\sigma_3}{\sigma_c} \right)^{1/\alpha} - m_b \frac{\sigma_3}{\sigma_c} - s = 0 \tag{14}$$

Substituting Equations (3)–(5) into Equation (14) gives:

$$\left(\frac{d\sigma_3}{\sigma_c} \right)^{\frac{1}{\frac{1}{2} + \frac{1}{6} \left(e^{-\frac{GSI}{15}} - e^{-\frac{20}{3}} \right)}} - \left(\frac{\sigma_3}{\sigma_c} \right) * m_i * e^{\frac{GSI-100}{28}} - \left(e^{\frac{GSI-100}{9}} \right) = 0 \tag{15}$$

5. Calculation Method

Equation (15) cannot be solved analytically, but it can be calculated numerically. The numerical solutions of Equation (15) for $\frac{\sigma_3^*}{\sigma_c}$ as a function of the GSI parameter were obtained using a custom-built program written in Matlab (The MathWorks Inc., Natick, MA, USA, MATLAB Version: 9.14.0 (R2023a)) scripts. In the data analysis, we only included those $\frac{\sigma_3^*}{\sigma_c}$ – GSI data pairs for which we found a unique real solution for a given GSI value. Our calculations were made for two different ductility parameters: 3.4 and 5.0 in cases of silicate and carbonate rocks, respectively, according to the suggestion of Walton [35]. The Geological Strength Index (GSI) ranges between 0 and 100, the m_i values were chosen to be quasi-uniform on a logarithmic scale. Figure 5 shows plots representing the generated numerical solutions of Equation (14) for various values of m_i , d , and Geological Strength Index (GSI). Here is an explanation of the conditions for each curve in the different parts of Figure 5:

Parts (a) and (b)—Semi-logarithmic Curves: These two plots depict the normalized confinement stress ($\frac{\sigma_3^*}{\sigma_c}$) as a function of GSI . Part (a): For $d = 3.4$ and Part (b): For $d = 5$.

Each light blue or red curve represents a different value of the material constant $m_i = (5, 7, 9, 12, 17, 24, 32, 45)$ which is a parameter of the Hoek–Brown failure criterion related to the material properties of the rock mass. Horizontal axis (GSI): Geological Strength Index, which represents the rock mass condition, ranging from 0 to 100. Vertical axis (logarithmic scale): Normalized confinement stress, plotted on a semi-log scale.

Part (c)—Residual Error Plots:

These two plots show the relative residuals between the numerical solution of Equation (15) and the model function (Equation (16)) as a function of GSI for the same two values of d as in (a) and (b):

- Left plot ($d = 3.4$);
- Right plot ($d = 5$);
- Horizontal axis: GSI values, ranging between 40 and 100;

- Vertical axis: Relative residual, which shows the difference between the actual numerical solution and the expected result from the equation.

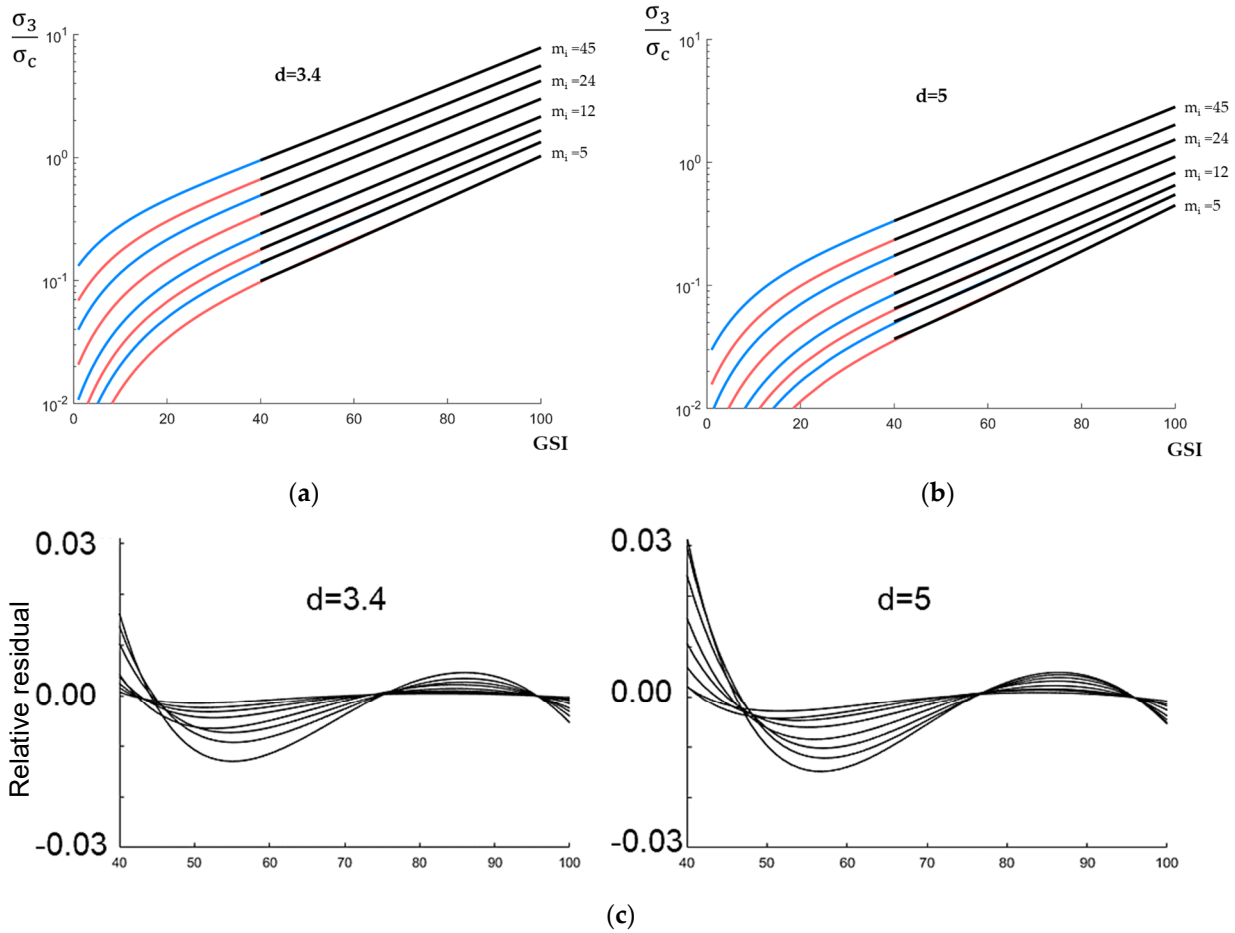


Figure 5. The generated numerical solution of Equation (14) is visualized (light blue and red solid lines) for different $\frac{\sigma_3^*}{\sigma_c} - GSI$ data pairs on a semi-logarithmic y -axis. For generation the data, we used $d_i = 3.4$ and $d_i = 5$, $m_i = (5, 7, 9, 12, 17, 24, 32, 45)$ and GSI between 0 and 100 (with an increment of 1). The shape of the decay of the curves with $GSI > 32$ clearly indicates a slope function on a logarithmic scale.

From the shape of the decay of the curves, we first deduced that the theoretical solution of Equation (15) with $GSI > 32$ approximately follows a straight line on a logarithmic scale, which, assuming a simpler function, indicates an exponential function. To approximate the shape of the solution function, then we fitted the generated curves (light blue and red solid lines in Figure 5a,b) with $y = a e^{b GSI} + c$ model. Then, we analyzed the effect of a , b , and c on the different m_i and d values. Assuming a simple functional form, we found that the solution of Equation (15) can be rewritten in the following form:

$$\frac{\sigma_3}{\sigma_c} = \alpha \frac{m_i}{d} e^{\beta \frac{d}{m_i} GSI} + \gamma \tag{16}$$

where α , β , and γ are constants values.

The generated curves for $GSI > 40$ were fitted with Equation (16), (solid black lines in Figure 5). The relative residuals between the model function (Equation (16)) and the numerical solution of Equation (16) are visualized in Figure 5c. The model function approximates the numerical solution with an accuracy of better than 3% in the investigated range.

6. Results and Discussion

Figure 6 presents four subplots (labeled as a, b, c, and d) that illustrate the relationship between the $(\frac{\sigma_3^*}{\sigma_c})$ and the Geological Strength Index (*GSI*) for different values of the material constant m_i and the ductility parameter d . Figure 6 uses a logarithmic scale for $(\frac{\sigma_3^*}{\sigma_c})$, and the *GSI* ranges from 0 to 100.

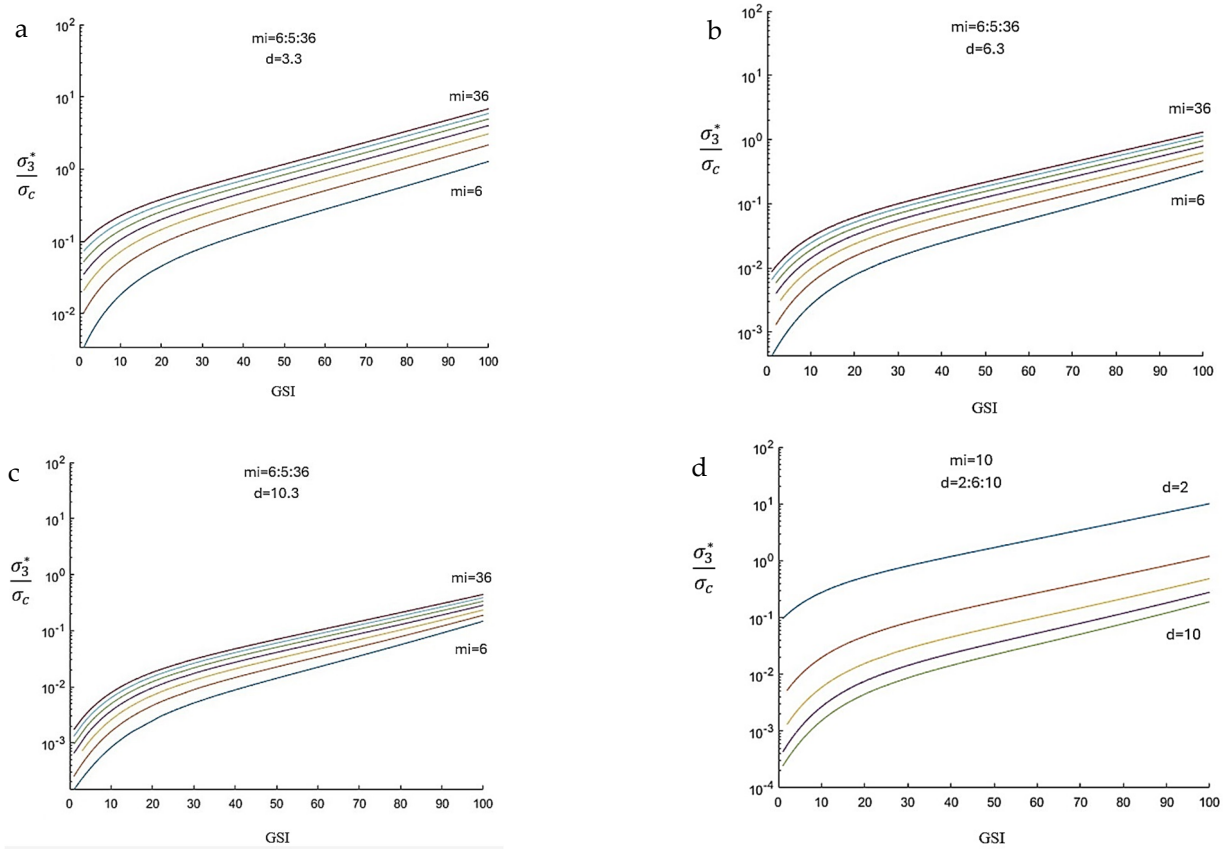


Figure 6. Relationship between $\frac{\sigma_3^*}{\sigma_c}$ and *GSI* for different values of Hoek–Brown (m_i) and Mogi ductility (d): (a) $d = 3.3$ and $m_i = 6:5:36$; (b) $d = 6.3$ and $m_i = 6:5:36$; (c) $d = 10.3$ and $m_i = 6:5:36$; (d) $m_i = 10$, $d = 2:2:10$ and $m_i = 10$.

- (a) As *GSI* increases, $(\frac{\sigma_3^*}{\sigma_c})$ also increases, but the rate of increase diminishes at higher *GSI* values. Higher m_i values result in higher $(\frac{\sigma_3^*}{\sigma_c})$ for the same *GSI*, indicating that rocks (with higher m_i) can sustain more confinement. The logarithmic scale indicates that the increase in $(\frac{\sigma_3^*}{\sigma_c})$ is exponential, but the difference between the curves becomes smaller at higher *GSI* values, suggesting a diminishing return in confinement strength with increasing *GSI*.
- (b) Similar trends are observed as in subplot (a), but with a slightly lower rate of increase in $(\frac{\sigma_3^*}{\sigma_c})$ for the same *GSI* and m_i values. The higher ductility parameter d (compared to subplot a) leads to lower overall $(\frac{\sigma_3^*}{\sigma_c})$ values, indicating that increased ductility reduces the rock mass’s ability to sustain confining pressure. The differences between the curves for different m_i values are still present but slightly reduced, especially at higher *GSI* values, compared to subplot (a).
- (c) This plot continues the trend of decreasing $(\frac{\sigma_3^*}{\sigma_c})$ values with increasing ductility parameter d . The curves are more closely spaced, especially at lower *GSI* values, indicating that the influence of m_i is less pronounced when the rock mass is more

- ductile. The exponential increase in $(\frac{\sigma_3^*}{\sigma_c})$ with GSI is still observed, but the effect of increasing m_i is less significant compared to the previous subplots.
- (d) This plot focuses on the effect of varying d with a fixed m_i value. As d increases, the curves shift downward, showing that increased ductility reduces the rock mass's ability to sustain confining pressure for any given GSI . The exponential relationship between $(\frac{\sigma_3^*}{\sigma_c})$ and GSI remains, but the curves for higher d values are significantly lower, emphasizing the negative impact of ductility on rock mass strength. The differences between the curves are more significant at higher GSI values, indicating that the impact of ductility is more pronounced in stronger rock masses.

In summary, this research focused on the brittle–ductile transition stress of rock mass by considering the effect of Geological Strength Index (GSI) values on the brittle–ductile transition stress of rock mass. To achieve this, the Hoek–Brown failure criteria for rock mass were reformulated mathematically, including the ductility parameter (d). The reformulated equation was solved numerically, and the relationship between $(\frac{\sigma_3^*}{\sigma_c})$ and Geological Strength Index (GSI) values was illustrated graphically and analyzed in different ranges.

7. Conclusions

In conclusion, this study offers a comprehensive analysis of the brittle–ductile transition in rock masses by integrating the Geological Strength Index (GSI) with the Hoek–Brown failure criterion. The research fills a significant gap in rock mechanics by focusing on the real-world complexities of rock masses, which contain discontinuities and heterogeneities, rather than solely on intact rocks. The results emphasize that GSI plays a pivotal role in the transition from brittle to ductile behavior, with higher GSI values corresponding to higher stress thresholds before ductile deformation occurs. This insight is critical for predicting how rock masses will respond to varying levels of confining stress.

The study further explores how the ductility parameter (d), derived from the ratio of differential stress to minor stress, affects the rock mass's ability to sustain confinement. The findings reveal an exponential relationship between brittle–ductile transition stress and GSI , demonstrating that rock masses with higher GSI values are capable of withstanding greater confinement stress. However, the effectiveness diminishes as GSI increases, suggesting diminishing returns in confinement strength for highly stable rock masses. The use of numerical solutions and models enhances the accuracy of predicting brittle–ductile transitions, offering engineers and geologists a practical tool for designing safe and efficient structures in tunneling, mining, and other underground constructions.

For instance, in tunneling projects through fault zones, like the Gotthard Base Tunnel in Switzerland, modeling helped predict when brittle failure would occur, preventing tunnel collapse by adapting support systems to handle brittle–ductile transitions. In deep mining operations, like those in the South African gold mines, understanding the brittle-to-ductile transition allows engineers to manage rockburst hazards more effectively. As rocks become more ductile at great depths, this reduces the risk of catastrophic brittle failures. Also, in underground storage reservoirs, like depleted gas fields, modeling this transition helps ensure the structural integrity of storage chambers. Preventing brittle failure in these chambers ensures stable gas containment over time.

Moreover, this research lays the groundwork for future studies, providing a framework for investigating the behavior of rock masses under extreme conditions. By incorporating factors like GSI and ductility, it also highlights the need for a more nuanced understanding of rock mass behavior, especially in critical engineering applications. These findings contribute to more effective design strategies and safer operations in the field of rock engineering, particularly in environments where predicting brittle failure or ductile flow is essential for stability and safety.

Author Contributions: Conceptualization, G.M. and S.M.D.; methodology, S.N.; software, G.M.; writing—original draft preparation, B.V. and S.M.D.; writing—review and editing, S.M.D. and B.V.; visualization, S.N.; supervision, B.V. All authors have read and agreed to the published version of the manuscript.

Funding: This research received no external funding.

Institutional Review Board Statement: Not applicable.

Informed Consent Statement: Not applicable.

Data Availability Statement: The original contributions presented in the study are included in the article, further inquiries can be directed to the corresponding author.

Conflicts of Interest: The authors declare no conflicts of interest.

List of Symbols

a	rock mass material constant (dependent on GSI)
d	ductility parameter
GSI	Geological Strength Index
m_b	Hoek–Brown material constant of rock mass (dependent on GSI)
m_i	Hoek–Brown material constant of intact rock
s	rock mass material constant (depend on GSI)
σ_1	major main stress
σ_3	minor main stress
σ_3^*	brittle–ductile transition stress
σ_c	unconfined compressive strength
σ_t	tensile strength

References

- Hetenyi, M. *Handbook of Experimental Stress Analysis*; Wiley: New York, NY, USA, 1966.
- Andreev, G.E. *Brittle Failure of Rock Materials: Test Results and Constitutive Models*; A.A. Balkema: Rotterdam/Brookfield, VT, USA, 1995.
- Yilmaz, N.G.; Karaca, Z.; Goktan, R.M.; Akal, C. Relative brittleness characterization of some selected granitic building stones: Influence of mineral grain size. *Constr. Build. Mater.* **2009**, *23*, 370–375. [[CrossRef](#)]
- Mogi, K. Pressure dependence of rock strength and transition from brittle fracture to ductile flow. *Bull. Earthq. Res. Inst.* **1966**, *44*, 215–232.
- Liu, Z.; Shao, J. Strength behavior, creep failure and permeability change of a tight marble under triaxial compression. *Rock Mech. Rock Eng.* **2017**, *50*, 529–541. [[CrossRef](#)]
- Yang, S.-Q.; Ju, Y.; Gao, F.; Gui, Y.-L. Strength, deformability and X-ray micro-CT observations of deeply buried marble under different confining pressures. *Rock Mech. Rock Eng.* **2016**, *49*, 4227–4244. [[CrossRef](#)]
- Wawersik, W.; Fairhurst, C. A study of brittle rock fracture in laboratory compression experiments. *Int. J. Rock Mech. Min. Sci. Geomech. Abstr.* **1970**, *7*, 561–575. [[CrossRef](#)]
- Reichmuth, D.R. Point load testing of brittle materials to determine tensile strength and relative brittleness. In Proceedings of the 9th US Symposium on Rock Mechanics (USRMS), Golden, CO, USA, 17–19 April 1967; pp. 134–159.
- Lawn, B.R.; Marshall, D.B. Hardness, toughness, and brittleness: An indentation analysis. *J. Am. Ceram. Soc.* **1979**, *62*, 347–350. [[CrossRef](#)]
- Dollinger, G.L.; Handewith, H.J.; Breeds, C.D. Use of the punch test for estimating TBM performance. *Int. J. Rock Mech. Mining Sci.* **1998**, *13*, 403–408. [[CrossRef](#)]
- Kármán, T. Mitől függ az anyag igénybevétele? (What influences the strength of the materials?). *Magyar Mérn. Egylet Közlönye* **1910**, *10*, 212–226. (In Hungarian)
- Kármán von, T. Festigkeits Versuche unter allseitigem Druck. *Z. Verhandl. Deut. Ingr.* **1911**, *55*, 1749–1759. (In German)
- Deák, F.; Ván, P.; Vásárhelyi, B. Hundred years after the first triaxial test. *Period. Polytech. Civ. Eng.* **2012**, *56*, 115–122. [[CrossRef](#)]
- Evans, B.; Fredrich, J.; Wong, T.F. The Brittle-Ductile Transition in Rocks: Recent Experimental and Theoretical Progress. In *The Brittle-Ductile Transition in Rocks*; Duda, A.G.U., Durham, W.B., Handin, J.W., Wang, H.F., Eds.; John Wiley & Sons: Hoboken, NJ, USA, 1990; Volume 56.
- Ledniczky, K.; Vásárhelyi, B. Brittle-ductile transition of anisotropic rocks during three-point bending test. *Acta Geod. Geoph. Hung.* **2000**, *35*, 75–80. [[CrossRef](#)]

16. Ván, P.; Vásárhelyi, B. Centenary of the first triaxial test—Recalculation of the results of Kármán. In *Eurock'2010 (Laussane), Rock Mechanics in Civil and Environment*; Zhao, J., Labiouse, V., Dubt, J.-P., Mathier, J.-F., Eds.; Taylor & Francis Group: London, UK, 2010; pp. 59–62.
17. Robertson, E.C. Experimental study of the strength of rocks. *Bull. Geol. Soc. Am.* **1955**, *66*, 1275–1314. [[CrossRef](#)]
18. Paterson, M.S.M.; Wong, T.-F. *Experimental Rock Deformation: The Brittle Field*; Springer: Berlin/Heidelberg, Germany, 2005.
19. Heard, H.C. Transition from brittle fracture to ductile flow in Solnhofen limestone as a function of temperature, confining pressure, and interstitial fluid pressure. In *Rock Deformation. Geology Society of America Memoirs*; Griggs, D., Handin, J., Eds.; Geological Society of America: McLean, VA, USA, 1960; pp. 193–226.
20. Byerlee, J.D. Brittle-ductile transition in rocks. *J. Geophys. Res.* **1968**, *73*, 4741–4750. [[CrossRef](#)]
21. Mogi, K. Fracture and flow of rocks. *Dev. Geotecton.* **1972**, *4*, 541–568.
22. Hoek, E.; Brown, E.T. Empirical strength criterion for rock masses. *J. Geotech. Eng. Div.* **1980**, *106*, 1013–1035. [[CrossRef](#)]
23. Wong, T.-f.; Baud, P. The brittle-ductile transition in porous rock: A review. *J. Struct. Geol.* **2012**, *44*, 25–53. [[CrossRef](#)]
24. Hoek, E.; Martin, C.D. Fracture initiation and propagation in intact rock—A review. *J. Rock Mech. Geotech. Eng.* **2014**, *6*, 278–300. [[CrossRef](#)]
25. Jacquey, A.B.; Cacace, M. Multiphysics modeling of a brittle-ductile lithosphere: 2. Semi-brittle, semi-ductile deformation and damage rheology. *J. Geophys. Res. Solid Earth* **2020**, *125*, 2019JB018475. [[CrossRef](#)]
26. O’Ghaffari, H.; Pec, M.; Mittal, T.; Mok, U.; Chang, H.; Evans, B. Microscopic defect dynamics during a brittle-to-ductile transition. *Proc. Natl. Acad. Sci. USA* **2023**, *120*, e2305667120. [[CrossRef](#)] [[PubMed](#)]
27. Tang, Y.; Sun, Y.; Zhu, Y.; Zhang, C.; Li, J. A unified hardening/softening elastoplastic model for rocks undergoing brittle-ductile transition with strength-mapping and fractional plastic flow rule. *Comput. Geotech.* **2024**, *173*, 106501. [[CrossRef](#)]
28. Aubertin, M.; Gill, D.E.; Simon, R. On the use of the brittleness index modified (BIM) to estimate the post-peak behavior of rock. In *Proceedings of the 1st North American Rock Mechanics Symposium, Austin, TX, USA, 1–3 June 1994*; pp. 945–952.
29. Meng, F.Z.; Zhou, H.; Zhang, C.; Xu, R.; Lu, J. Evaluation methodology of brittleness of rock based on post-peak stress-strain curves. *Rock Mech. Rock Eng.* **2015**, *48*, 1787–1805. [[CrossRef](#)]
30. Zhang, L.M.; Cong, Y.; Meng, F.Z.; Wang, Z.Q.; Zhang, P.; Gao, S. Energy evolution analysis and failure criteria for rock under different stress paths. *Acta Geotech.* **2021**, *16*, 569–580. [[CrossRef](#)]
31. Gong, F.Q.; Yan, J.Y.; Song Luo, S.; Li, X.B. Investigation on the linear energy storage and dissipation laws of rock materials under uniaxial compression. *Rock Mech. Rock Eng.* **2019**, *52*, 4237–4255. [[CrossRef](#)]
32. Hoek, E.; Brown, E.T. *Underground Excavations in Rock*; Institution of Mining and Metallurgy: London, UK, 1980.
33. Eberhardt, E. The Hoek–Brown failure criterion. *Rock Mech. Rock Eng.* **2012**, *45*, 981–988. [[CrossRef](#)]
34. Hoek, E.; Brown, E.T. The Hoek–Brown failure criterion and GSI: 2018 edition. *J. Rock Mech. Geotech. Eng.* **2019**, *11*, 445–463. [[CrossRef](#)]
35. Walton, G. A new perspective on the brittle-ductile transition of rocks. *Rock Mech. Rock Eng.* **2021**, *54*, 5993–6006. [[CrossRef](#)]
36. Davarpanah, S.M.; Sharghi, M.; Narimani, S.; Török, Á.; Vásárhelyi, B. Brittle-ductile transition stress of different rock types and its relationship with uniaxial compressive strength and Hoek–Brown material constant (mi). *Sci. Rep.* **2023**, *13*, 1186. [[CrossRef](#)] [[PubMed](#)]
37. Davarpanah, S.M.; Sharghi, M.; Vásárhelyi, B.; Török, Á. Characterization of Hoek–Brown constant mi of quasi-isotropic intact rock using rigidity index approach. *Acta Geotech.* **2022**, *17*, 877–902. [[CrossRef](#)]

Disclaimer/Publisher’s Note: The statements, opinions and data contained in all publications are solely those of the individual author(s) and contributor(s) and not of MDPI and/or the editor(s). MDPI and/or the editor(s) disclaim responsibility for any injury to people or property resulting from any ideas, methods, instructions or products referred to in the content.